

ISO SPECTROSCOPY OF THE HH 7-11 FLOW AND ITS RED-SHIFTED COUNTERPART⁰

SERGIO MOLINARI AND ALBERTO NORIEGA-CRESPO

Infrared Processing and Analysis Center & SIRTf Science Center, California Institute of Technology, MS 100-22,
Pasadena, CA 91125, USA

CECILIA CECCARELLI

Laboratoire d'Astrophysique, Observatoire de Grenoble - BP 53, F-38041 Grenoble cedex 09, France

BRUNELLA NISINI, TERESA GIANNINI AND DARIO LORENZETTI

Osservatorio Astronomico di Roma, via Frascati 33, I-00044 Monte Porzio, Italy

EMMANUEL CAUX

CESR CNRS-UPS, BP 4346, F-31028 Toulouse Cedex 04, France

RENÉ LISEAU

Stockholm Observatory, S-133 36 - Saltsjöbaden, Sweden

PAOLO SARACENO

CNR-Istituto di Fisica dello Spazio Interplanetario, Area di Ricerca Tor Vergata, via Fosso del Cavaliere I-00133 Roma,
Italy

GLENN J. WHITE

Department of Physics, Queen Mary and Westfield College, University of London, Mile End Road, London E1 4NS, UK
Stockholm Observatory, S-133 36 - Saltsjöbaden, Sweden

Accepted 2000 February 29

ABSTRACT

We have used the two spectrometers on the Infrared Space Observatory to observe the HH 7-11 flow, its red-shifted counterpart, and the candidate exciting source SVS 13, in the star formation region NGC 1333. We detect atomic ([OI]63 μ m, [OI]145 μ m, [SiII]34.8 μ m, [CII]158 μ m) and molecular (H₂, CO, H₂O) lines at various positions along the bipolar flow.

Most of the observed lines can be explained in terms of shock-excited emission. In particular, our analysis shows that dissociative (J-type) and non-dissociative (C-type) shocks are simultaneously present everywhere along both lobes of the flow. We confirm the low-excitation nature of the Herbig-Haro nebulosities, with shock velocities $v_s \lesssim 40 - 50$ km s⁻¹. Toward both lobes of the outflow we find pre-shock densities of $n_0 \sim 10^4$ cm⁻³ for both the J and C components, implying $B_0 \sim 100 \mu$ G for $B_0 \propto n_0^{0.5}$. In the central region of the flow, close to the exciting source, the pre-shock density deduced for the C-shock component is $n_0 \sim 10^5$ cm⁻³, suggesting a magnetic field ~ 3 times stronger. We propose that the deficiency of gas-phase water in the post C-shock regions is due to freezing onto warm grains processed through the J-shock front and traveling along the magnetic field lines. The total observed cooling from the dissociative shock components is consistent with the power lost by a slow molecular outflow accelerated by a fast neutral HI wind.

Finally, the skin of the cloud seen in projection toward the flow appears to be weakly photo-ionised by BD +30° 549, the dominant illuminating source of the NGC 1333 reflection nebula.

Subject headings: Stars: formation - (ISM:) Herbig-Haro objects - ISM: individual objects: HH 7-11 - ISM: molecules - Infrared: ISM: lines and bands

⁰Based on observations with ISO, an ESA project with instruments funded by ESA Member States (especially the PI countries: France, Germany, the Netherlands and the United Kingdom) with the participation of ISAS and NASA.

1. INTRODUCTION

Atomic and molecular outflows trace the mass loss from protostellar objects, which is a fundamental characteristic of the formation and evolution of low mass stars. These outflows are often traced by the optical Herbig-Haro (HH) objects, shock-excited nebulosities which mark the interface between outflowing and circumstellar material. One of these systems, which since its discovery (Herbig 1974 ; Strom et al. 1974) has been subjected to a detailed multi-wavelength analysis, is HH 7-11. The system is relatively bright and lies in the very active star forming NGC 1333 region (Aspin et al. 1994; Bally et al. 1996). A distance to the outflow of 350pc (Herbig & Jones 1983) is widely adopted in the literature, although Cernis (1993) proposes 200pc. Early optical spectroscopic studies show that the HH 7-11 outflow has a complex velocity field and low excitation (Solf & Böhm 1987; Böhm & Solf 1990), a conclusion further supported by near infrared studies (Hartigan et al. 1989; Carr 1993). Early on, a well defined CO bipolar outflow was detected associated with this system (Snell & Edwards 1981; Bachiller & Cernicharo 1990), which also is observed in some other molecules like HCO⁺ and H₂O (Mehring 1996; Cernicharo et al. 1996).

The HH 7-11 outflow has an unusual morphology; the blue outflow lobe is made up of an arc-shaped chain of knots, while the red one is invisible at optical wavelengths. The red lobe is, however, detected in the (1-0)S(1) H₂ line at 2.12 μ m having a very ragged appearance (see Fig 1). Both lobes have a total extension of $\sim 2'$. It has been thought that the driving source of the outflow is the infrared star SVS 13 (Strom et al. 1976), a conclusion partially supported by the proper motion measurements of the knots (Herbig & Jones 1983) and the source observed outbursts (Goodrich 1986; Eislöffel et al. 1991; Liseau et al. 1992). The source has a luminosity of $\sim 85 L_{\odot}$ (Molinari et al. 1993). Recent high angular resolution ($\sim 0.''3$) VLA continuum observations at 3.6 cm suggest another nearby embedded source (VLA 3) as a likely candidate, based on its better alignment with the HH string. Interferometric observations (Bachiller et al. 1998) at 1.3 and 3.5 mm with better than 0.''2 resolution, however, have not confirmed this. The interferometric observations have led to the discovery of a second jet

emanating from a more deeply embedded source 14.''5 away from SVS 13, named SVS 13B (Grossman et al. 1987).

One of the reasons why the HH 7-11 flow has been so intensively studied (see e.g. Reipurth 1994), is that it was the first system showing clear signatures of a high velocity outflow in both neutral and molecular gas tracers (Lizano et al. 1988; Rodriguez et al. 1990; Giovannardi et al. 1992). This was a major step forward in the interpretation of molecular outflows as being driven by faster but more tenuous (than the outflow entrained gas) atomic stellar winds (Masson & Chernin 1993; Raga et al. 1993). This has led to a more careful analysis of the energetics and shock conditions associated with the ionic/atomic and molecular gas outflows (Raga 1991). HH 7-11 is also one of the few examples where it is possible to disentangle the contributions of shock excited and fluorescent emission from its near infrared H₂ spectra (Gredel 1996; Fernandes & Brand 1995; Everett 1997).

In the present study, we take advantage of the capabilities of the Infrared Satellite Observatory (ISO, Kessler et al. 1996) spectrometers to study the mid- and far infrared emission line spectra from the HH 7-11 red and blue lobes and around the driving source SVS 13. The observations are described in Sect. 2; the results are presented and discussed in Sect. 3 and following, and the main conclusions are summarised in Sect. 9.

2. OBSERVATIONS AND DATA REDUCTION

We used the two spectrometers on the ISO satellite to observe several locations along the HH 7-11 flow, its optically invisible counterflow and the candidate exciting source SVS 13. The Long Wavelength Spectrometer (LWS, Clegg et al. 1996) was used in its LWS01 grating mode to acquire full low resolution ($R \sim 200$) 43-197 μ m scans with data collected every 1/4 of a resolution element (equivalent to $\sim 0.07\mu$ m for $\lambda \lesssim 90\mu$ m, and to $\sim 0.15\mu$ m for $\lambda \gtrsim 90\mu$ m); a total of 19 scans were collected, corresponding to 38s integration time per spectral element. The LWS was also used in LWS04 Fabry-Perot (FP) mode to collect high ($R \sim 8000$) resolution scans of the [O I]63 μ m line; 52 scans sampled at 1/4 of the resolution element (i.e., $\sim 0.0017 \mu$ m, or 8 km s⁻¹) were collected, equivalent to an integration time of ~ 100 s per spectral element. The Short Wavelength Spectrometer (SWS, de Graauw et

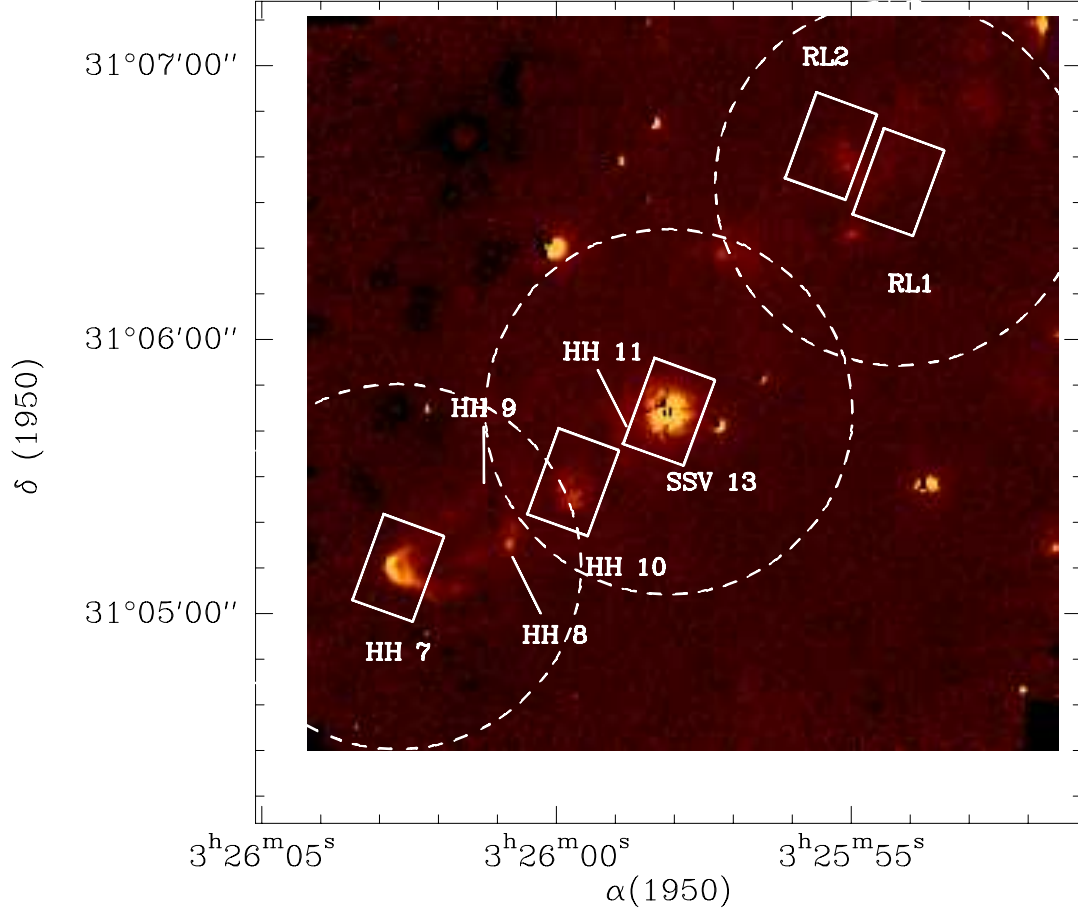


FIG. 1.— ISO fields of view in the various observed positions, superimposed onto a continuum-subtracted H_2 (1-0)S(1) line map. The dashed circles and solid rectangular apertures represent the LWS and SWS fields of view centered on the various observed positions. SSV 13 is at the center of the middle LWS (dashed circle) field of view.

TABLE 1

Observations

Object	$\alpha(1950)$	$\delta(1950)$	AOT	Rev	Obs. Time
SVS 13	03 25 58.1	+31 05 44.1	LWS01	654	4053
			SWS02	814	1730
HH 7	03 26 02.7	+31 05 10.2	LWS01	654	3165
			LWS04	831	2428
			SWS02	652	1464
HH 10	03 25 59.8	+31 05 28.8	SWS02	847	1730
Red Lobe 1 (RL 1)	03 25 54.3	+31 06 34.1	LWS01 ^a	654	3165
			LWS04 ^a	831	2428
			SWS02	652	1464
Red Lobe 2 (RL 2)	03 25 55.4	+31 06 42.1	SWS02	847	1730

^a The field of view also includes the position “Red Lobe 2”

al. 1996) was used in its SWS02 grating mode to observe line scans at medium resolution ($R \sim 2000$) for selected wavelength regions covering the [SiII]34.8 μm and [NeII]12.8 μm fine structure lines, and the pure rotational transitions of molecular hydrogen from (0-0)S(1) to (0-0)S(7). All relevant information is summarised in Table 1, including the Astronomical Observation Templates used, the revolution number and the total observing time of the observations.

LWS data processed through Off-Line Processing (OLP), version 7, have been reduced using the LWS Interactive Analysis¹ (LIA) Version 7.2. The dark current and gain for each detector were re-estimated, and the data were recalibrated in wavelength, bandpass and flux. The absolute flux calibration quoted for LWS in grating mode is 10-15% and it is valid for point-like sources since the primary calibrator, Uranus, is point-like to the LWS beam; however, our sources are not rigorously point-like and we adopt a more conservative number of 20%. Additional processing for the FP data (with the LIA routine FP_PROC) included a gain correction to compensate for the incorrect positioning of the grating during the FP observations. The integrated [OI]63 μm line fluxes obtained with the FP are about a factor of 2 lower than the values measured using the grating. This discrepancy is larger than the 30% figure generally quoted for the absolute flux calibration of the FP (Swinyard et al 1998). We cannot offer any explanation for this difference, and in this paper we will not use the line fluxes measured with the FP. The accuracy of the FP wavelength calibration is believed to be better than 1/2 resolution element, or $\sim 15 \text{ km s}^{-1}$.

SWS data were processed using OSIA, the SWS Interactive Analysis². Dark currents and photometric checks were revised; in many cases the former were corrupted on a few detectors and were re-estimated and subtracted. The March 1998 bandpass calibration files have been used to produce the final spectra. The absolute flux calibration for SWS data should be accurate to within 20%.

The final steps of data analysis were done using the ISO Spectral Analysis Package³ (ISAP) Version 1.5 for both LWS and SWS. Grating

scans (LWS) and detectors spectra (SWS) were averaged using a median clipping algorithm optimised to flag and discard outliers mainly due to transients; line fluxes were estimated by means of gaussian fitting (multiple gaussians in case of blended lines). The LWS observations toward HH 7 and the red lobe (RL 1+2) were heavily fringed due to the vicinity of the relatively strong continuum source SVS 13; standard techniques available under ISAP were used to remove these instrumental effects.

The locations of the observed positions and instrument apertures are shown in Fig. 1 superimposed on an H₂ (1-0)S(1) 2.12 μm continuum-subtracted map obtained with the near infrared camera at the 60" Mt. Palomar telescope (Murphy et al. 1995). The apertures of the two ISO spectrometers are quite different. The SWS focal plane aperture is 14"x20" for all of the detected lines except for [SiII]34.8 μm (20"x33") so that, at each pointing, the contamination from nearby knots should be negligible. The LWS aperture is rather large ($\varnothing \sim 80''$, Swinyard et al. 1998); the pointing on SVS 13 also includes HH 11 and 10 and two sources VLA 3 and SVS 13B (see Sect. 1), while that centered on HH 7 also includes HH 8, 9 and 10.

3. RESULTS

Table 2 presents the fluxes for the lines detected toward each location. One sigma upper limits are given only for lines observed with dedicated SWS02 "line scans" AOTs but not detected (see Tab. 1); a horizontal dash means that no observation is available for that particular line.

Detected lines are also plotted in Figs. 2a, b, c and d; most of them are detected everywhere. Exceptions are [SiII]34.8 μm , which is not detected toward RL 2, *ortho*-H₂O which is not detected toward RL 1+2, and [NeII]12.8 μm which is not detected anywhere. All lines, except [SiII]34.8 μm and the H₂ lines, are stronger on the SVS 13 position.

The FP spectra of the [OI]63 μm line toward HH 7 and RL 1+2 are presented in Fig. 3. The lines are resolved ($\Delta v_{FP} \sim 30 \text{ km s}^{-1}$) with deconvolved FWHM of $\sim 50 \text{ km s}^{-1}$ and $\sim 25 \text{ km s}^{-1}$ for the two positions; these widths are consistent with the velocity field traced by the [S II]6717Å

¹LIA is available at <http://www.ipac.caltech.edu/iso/lws/lia/lia.html>

²OSIA is available at http://www.mpe.mpg.de/www_ir/ISO/observer/osia/osia.html

³ISAP is available at <http://www.ipac.caltech.edu/iso/isap/isap.html>

TABLE 2
Observed Line Fluxes^a

Line	SVS 13	HH 7	HH 10	Red Lobe 1	Red Lobe 2
SWS Lines					
(0-0)S(1) ^d	4.0(0.5)	2.6(0.5)	5.5(0.5)	4.5(0.7)	4.2(0.5)
(0-0)S(2) ^e	7.9(2.6)	13.3(1.9)	6.9(1.2)	7.6(2.1)	8.3(2.5)
(0-0)S(3) ^e	9.3(0.8)	10.2(0.7)	12.5(1.1)	10.6(0.9)	7.8(0.8)
(0-0)S(4) ^e	4.2(0.6)	10.9(1.0)	5.3(0.6)	4.2(0.8)	3.1(0.7)
(0-0)S(5) ^e	9.9(2.0)	15.5(1.9)	9.9(1.5)	8.7(2.0)	11.9(2.4)
(0-0)S(6) ^e	≤2	—	≤3	—	≤3
(0-0)S(7) ^e	≤4	—	≤5	—	≤5
[NeII]12.8 μm^{d}	≤0.7	≤0.9	≤0.7	≤0.9	≤0.8
[SiII]34.8 μm^{g}	7.4(2.3)	3.6(1.1)	6.8(2.2)	5.5(1.0)	≤3
LWS Lines					
CO 20-19 ^f	5.4(1.7) ^b	—	—	—	—
CO 19-18 ^f	13.7(2.0) ^b	—	—	—	—
CO 18-17 ^f	13.0(4.6) ^b	—	—	—	—
CO 17-16 ^f	10.1(1.7) ^b	8.4(3.0) ^c	—	6.6(1.2)	—
CO 16-15 ^f	10.1(1.7) ^b	5.7(1.5) ^c	—	3.9(0.6)	—
CO 15-14 ^f	13.2(6.3) ^b	8.5(2.8) ^c	—	—	—
CO 14-13 ^f	10.1(2.7) ^b	6.6(2.1) ^c	—	—	—
o-H ₂ O 3(0,3)-2(1,2) ^f	12.2(6.3) ^b	6.5(2.8) ^c	—	—	—
o-H ₂ O 2(1,2)-1(0,1) ^f	6.8(3.8) ^b	7.9(1.5) ^c	—	—	—
[OI]63 μm^{f}	180(2) ^b	131(3) ^c	—	109(3)	—
[OI]145 μm^{f}	8.0(4.0) ^b	4.6(1.0) ^c	—	7.9(1.3)	—
[CII]158 μm^{f}	21.3(1.4) ^b	12.5(1.1) ^c	—	15.2(0.7)	—

^a Units of 10^{-20} W cm^{-2} and 1σ uncertainties in parenthesis; upper limits are at the 1σ level.

A horizontal dash means that no observation is available for that particular line.

^b Includes HH 10 and HH 11.

^c Includes HH 8 and; HH 9 and HH 10 are at the edge of the LWS beam.

^d Focal plane aperture is $14'' \times 27''$.

^e Focal plane aperture is $14'' \times 20''$.

^f Focal plane aperture radius is $40''$.

^g Focal plane aperture is $20'' \times 33''$.

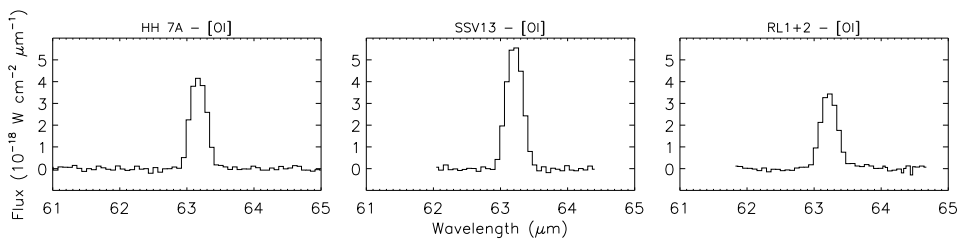


FIG. 2.— **a.** [OI]63 μm lines detected in the LWS full grating scans on the three observed positions (dashed circles in Fig. 1).

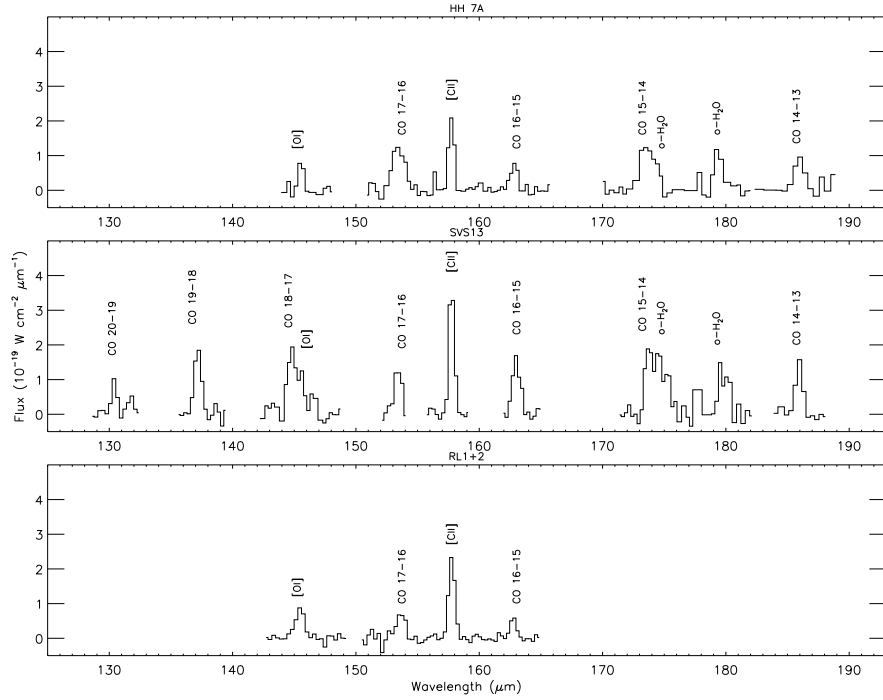


FIG. 2.— **b.** Lines detected between $130\mu\text{m}$ and $190\mu\text{m}$ in the LWS full grating scans on the three observed positions (dashed circles in Fig. 1).

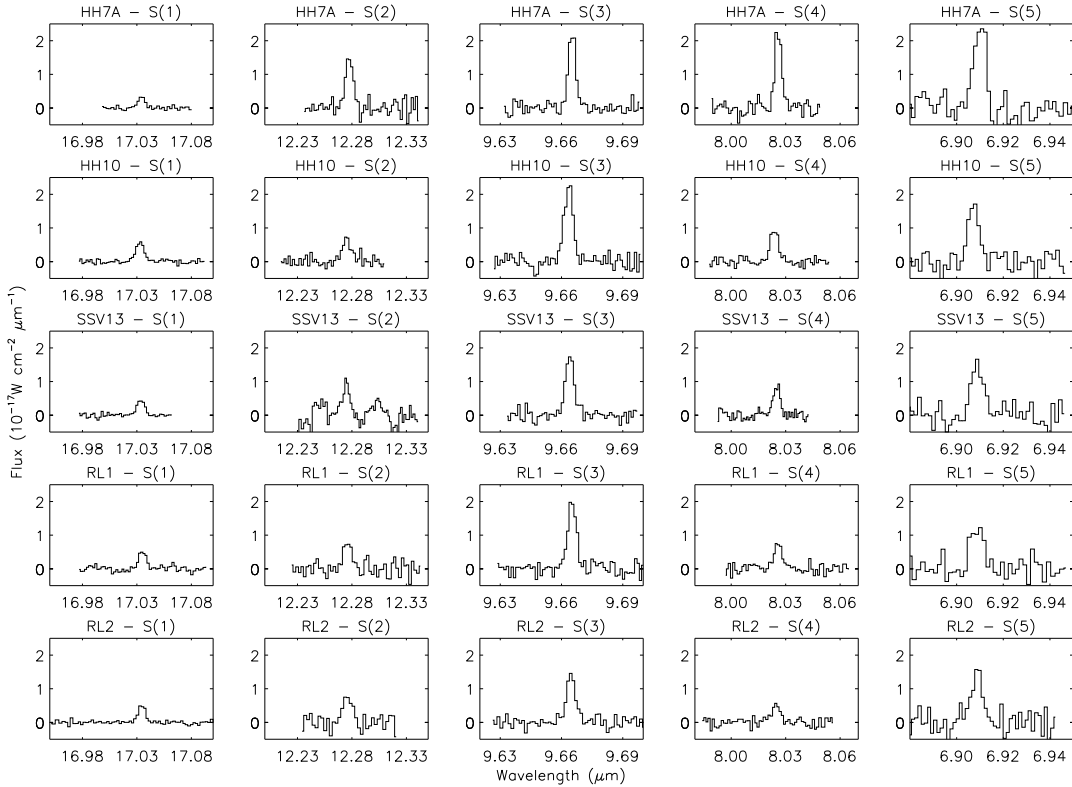


FIG. 2.— **c.** H₂ pure rotational lines detected in the SWS line grating scans on the five observed positions (full rectangles in Fig. 1).

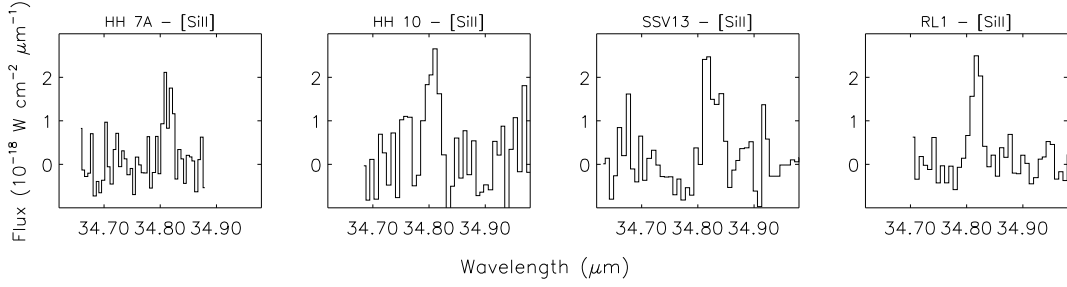


FIG. 2.— **d.** [SiII]34.8 μ m lines detected in the SWS line grating scans on four out of five observed positions (full rectangles in Fig. 1).

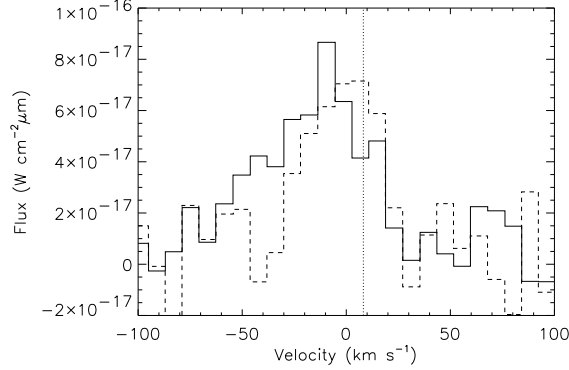


FIG. 3.— [OI]63 μ m line detected with the LWS Fabry-Perot toward HH 7 (full line) and RL 1+RL 2 (dashed line); the dotted vertical line indicates the cloud systemic velocity, 8.3 km s⁻¹.

line (Stapelfeldt 1991) toward HH 7, and suggest that [OI]63 μ m originates from the flow material.

4. THE GAS PHYSICAL PARAMETERS

4.1. H₂

The observed H₂ lines arise from quadrupole rotational transitions of the ground vibrational state so that they are likely to be optically thin. The radiative lifetimes range from 0.54 yrs for level $v=0$, $J=7$ where line (0-0)S(5) originates, to ~ 1000 yrs for level $v=0$, $J=2$ which is the upper state for (0-0)S(0) transition; thus these levels are collisionally populated, and a simple LTE analysis is adequate to interpret the data (e.g., Gredel 1994). Einstein coefficients and wavenumbers were taken from Black & Dalgarno (1976) and Dabrowski (1984); ortho/para=3 has been assumed. We dereddened the H₂ line fluxes using the visual extinction given by Gredel (1996) for the individual HH knots, and the Rieke & Lebofsky (1985) extinction curve. Dereddened line fluxes were used to produce the Boltzmann plots shown in Fig. 4; a single temperature fit is

in good agreement with the observed fluxes at all positions. The solid angles of line emitting regions are arbitrarily set to the equivalent SWS focal plane aperture, i.e. 14" x 20" or 6.6×10^{-9} sr (valid for all detected H₂ lines but S(1), where the solid angle is $\sim 30\%$ higher), assuming a beam filling factor of 1.

The H₂ temperatures and the SWS beam averaged column densities, together with 1σ uncertainties are listed in Table 3. The H₂ column densities should be considered as lower limits because the beam filling factor can be less than 1. The H₂ temperatures vary by less than 15% along the flow and appear to trace an H₂ component (which we call “warm”) which is colder than the one identified by Gredel (1996) via higher excitation H₂ ro-vibrational lines ($2100 \text{ K} \leq T \leq 2750 \text{ K}$, which we will call “hot”). The column densities for the warm H₂ (see Table 3, col. 3) are on average two orders of magnitude higher than those of the hot H₂ (Gredel 1996) and the difference cannot be explained by the smaller (a factor 2) emitting areas adopted by Gredel⁴. This suggests that the two

⁴We believe that Table 3 of Gredel (1996) incorrectly reports the H₂ column densities; based on the explanation in note *c* of that Table, the total column densities should be a factor ten higher than reported in its column 7. Furthermore (R. Gredel, priv. comm.) the IRSPEC slit was not aligned exactly on the peaks of the individual knots, suggesting that

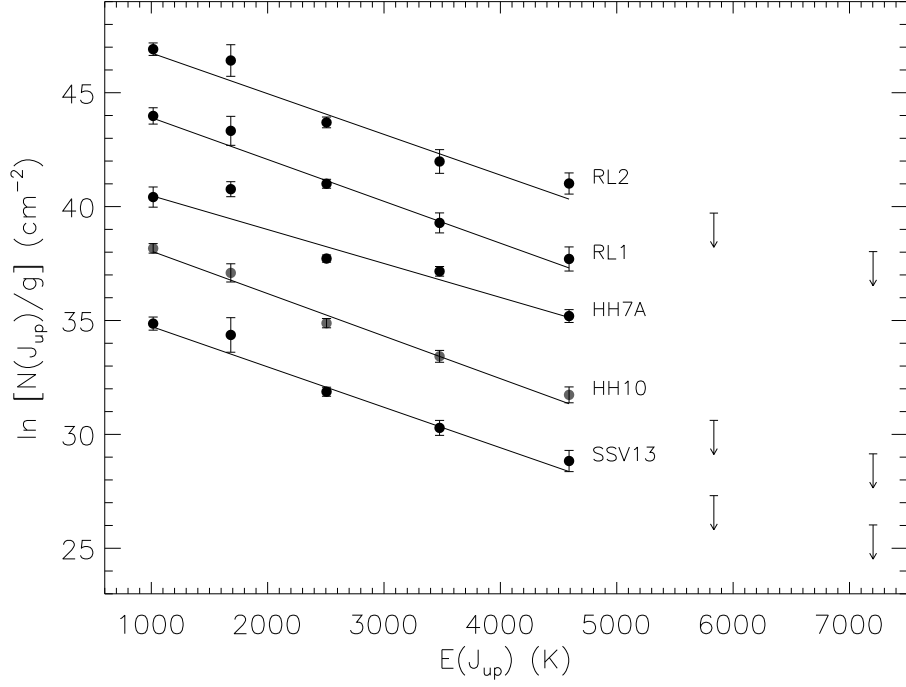


FIG. 4.— H_2 excitation diagrams for the five observed positions. In each panel, the abscissa represents the energy of the level in K, while N_j/g_j is in ordinata; offsets of -10, -5, 5 and 10 dex have been applied to data of SSV 13, HH 10, RL 1 and RL 2 while no offset has been applied to the HH 7 data.

TABLE 3

H_2 Physical Parameters

Object	T_{H_2} (K)	$N(\text{H}_2)$ (10^{20} cm^{-2})
SVS 13	560(20)	0.7(0.1)
HH 7	670(20)	0.5(0.1)
HH 10	540(10)	1.0(0.1)
RL 1	540(20)	0.9(0.2)
RL 2	560(20)	0.8(0.1)

H₂ components may be actually distinct.

4.2. CO

CO rotational lines have been detected at all three positions observed with LWS, although the intensity and number of detected lines are highest toward SVS 13. More CO lines than those reported in Table 2 are marginally visible in our spectra toward the two flow positions, but it is impossible to reliably determine their flux because of the heavily fringed LWS spectra. Contrary to the H₂ lines, the CO rotational spectrum arises from dipole transitions and the simplifying assumptions of optically thin lines cannot be adopted *a priori*. We analysed the CO lines using the LVG model described in Ceccarelli et al. (1998). Under NLTE conditions the line ratios depend both on the gas temperature and density, as well as on the CO column density if the lines are optically thick. The observed CO lines cannot constrain the three parameters simultaneously. The distribution of CO line fluxes *vs* J toward SVS 13 is essentially flat, and we find a range of physical conditions which are consistent with our observations. We find, as extreme cases, a ‘cold’ solution with $T \sim 350$ K and $n \sim 10^6$ cm⁻³, and a ‘warm’ solution with $T \sim 900$ K and $n \sim 10^5$ cm⁻³; the model also predicts optically thin CO lines. Interestingly, this temperature range is centered around the value independently derived from H₂ lines, which suggests that the CO and H₂ emission come from the same region. For $T = 560$ K (the H₂ temperature toward SVS 13, see Table 3) we obtain $n \sim 4 \times 10^5$ cm⁻³. The CO line ratios toward HH7 and RL 1+2 imply temperatures and densities similar to those around SVS 13, although the lower absolute line fluxes would suggest column densities or beam filling factor about a factor two lower. Using the SWS beam solid angle we derive $N(\text{CO}) \sim 2 \times 10^{16}$ cm⁻² toward the SVS 13 LWS pointing, giving a *direct* measurement of the CO abundance in this warm gas of $[\text{CO}]/[\text{H}] \sim 1.2 \times 10^{-4}$. Based on this number it seems that CO accounts for essentially all of the gas-phase carbon in the interstellar medium (Cardelli et al. 1996). Recently Lefloch et al. (1998) found evidence of CO depletion toward the core of SVS 13, likely due to condensation onto grains in the dense environments close to SVS 13. We find no evidence of such a depletion in the high-J CO line emitting region, suggesting that quoted column densities should more conservatively be considered as lower limits.

all of the CO locked into the grain mantles has been returned to the gas-phase.

4.3. H₂O

As far as H₂O is concerned, since only the 3(0,3)-2(1,2) 174.6 μm and 2(1,2)-1(0,1) 179.5 μm lines of *ortho*-H₂O have been detected in SVS 13 and HH 7, it is clear that water plays only a secondary role in gas cooling (see Table 4) compared to some other cases of outflow exciting sources such as IC 1396N (Molinari et al. 1998) or L1448-mm (Nisini et al. 1999). This result goes against earlier suggestions based on previous $\lambda = 1.67$ mm water line observations (Cernicharo et al. 1996), that the emission originates in dense (10^6 cm⁻³) shocked material with a water abundance comparable to that of CO. It should be noted, however, that Cernicharo et al. assumed a gas temperature of 50 K, while our observations of H₂ and CO lines clearly indicate that the temperature of the molecular material is a factor of 10 higher. The maps presented by Cernicharo et al. show that water emission is concentrated within $\sim 10''$ region centered on HH 11. Adopting $T = 560$ K and $n = 4 \times 10^5$ cm⁻³, compatible with the conditions for H₂ and CO, our model fit (Ceccarelli et al. 1998) to ISO and millimeter water lines predicts optically thick lines and a water column density $N(\text{H}_2\text{O}) \sim 10^{15}$ cm⁻², about a factor 20 lower than that estimated by Cernicharo et al. An abundance $[\text{H}_2\text{O}]/[\text{H}_2] \lesssim 6 \times 10^{-6}$ is also derived assuming that the lines from two molecules come from the same gas component; we will prove this assumption in Sect. 6.

5. THE PHOTO-DISSOCIATION REGION

In spite of the shock-excited nature of the HH objects, it is likely that a non-negligible contribution to the observed line emission actually come from an extended Photo-Dissociation Region (PDR, Tielens & Hollenbach 1985) component associated with the NGC 1333 cloud. This is suggested by low dispersion ISO-LWS observations (Caux et al. 2000) at various positions in the NGC 1333 cloud, which show a widespread [OI]63 μm and [CII]158 μm emission; this extended component seems to account for $\sim 20\%$ of the [OI]63 μm, and all of the [CII]158 μm emission we see from our LWS pointings. Our FP data (Sect. 3) confirm that only a small fraction of the

[OI]63 μ m line may come from a quiescent PDR component.

Using the *PDR Toolbox*⁵, the observed [CII]158 μ m emission requires a relatively faint FUV irradiation level of $G_0 \lesssim 10$ in units of local Galactic FUV flux (Habing 1968). Although SVS 13 might be able to provide the required FUV field, the widespread [CII]158 μ m emission seen by Caux et al. (2000) clearly suggest an external irradiation source. A natural candidate is BD +30° 549, the B6 star responsible for the illumination of the NGC 1333 reflection nebula (Harvey et al. 1984); located ~ 0.8 pc N-NE of the HH 7-11 area, it can certainly provide the needed $G_0 \lesssim 10$ FUV field. In this regime, the PDR surface temperature does not exceed ~ 100 K (Kaufman et al. 1999, Timmermann et al. 1996, Kemper et al. 1999, Liseau et al. 1999) which excludes a PDR origin for the [SiII]34.8 μ m line (Hollenbach, Takahashi & Tielens 1991), the H₂ and the CO lines. Indeed, the temperature of the molecular material is at least 5 times higher, and the molecular emission does not appear to be extended as one would expect for a PDR origin; ISOCAM-CVF near-IR imaging spectroscopy of the HH 7-11 region extracted from the public ISO data archive⁶ shows that the emission from the same H₂ rotational lines observed with SWS is concentrated along the flow and peaks in correspondence of visible HH objects (Noriega-Crespo et al. 2000), obviously favouring a shock origin for these lines.

6. SHOCKS ALONG THE FLOW

It is known that the nature of the shock excitation is dramatically influenced by the presence of a magnetic field component perpendicular to the shock velocity which prepares the up-stream medium and smoothes out the effect of the front passage. The differences in the physical conditions of shocked gas are such that two distinct classes of shocks, *C(ontinuous)* and *J(ump)* have been idealised (Draine 1980). In a J-shock the temperature reached by the shocked material depends on the square of the shock velocity and can

be as high as 10^5 K, resulting in complete molecular dissociation. In C-shocks, the temperature rarely exceeds a few thousand degrees and molecular material can survive. These two very different physical scenarios produce distinctive signatures in terms of cooling ratios between different species, and of line ratios within the same species. We will show that our data of the HH 7-11 region depict a complex situation where the two types of shock coexist; to help the discussion below, we report in Table 4 the total cooling rates in the various species as, when applicable, derived from the models used to estimate their physical parameters.

6.1. *J-shocks*

First of all we note that the non-detection of the [NeII]12.8 μ m line down to a level of 10^{-20} W cm⁻² confirms the low-excitation nature of the HH 7-11 chain and suggests (Hollenbach & McKee 1989, hereafter HM89) a shock velocity $v_s \lesssim 40 - 50$ km s⁻¹, depending of the pre-shock density, in excellent agreement with our high-resolution FP [OI]63 μ m observations (Sect. 3) and with estimates from optical spectroscopy (Böhm, Brugel & Olmsted 1983; Solf & Böhm 1987). This upper limit on the shock velocity excludes strong shocks, yet the detection of [SiII]34.8 μ m requires the presence of a dissociative shock component, since negligible ionization is expected from a C-shock (HM89). Such a component would also explain the observed [OI]63 μ m cooling, since the latter is expected to be the main coolant in J-shocks⁷. In order to compare the [OI]63 μ m with the [SiII]34.8 μ m line for HH 7 and SVS 13, we need to determine the fraction of [OI]63 μ m emission due to other HH objects falling within the LWS beam.

The LWS beam centered on HH 7 also contains HH 8, 9 and 10; since the excitation conditions for the different HH objects along the flow do not show dramatic variations (Hartigan, Curiel & Raymond 1989), we choose to use the detected [SiII]34.8 μ m lines toward HH 7 and HH 10

⁵The “*PDR Toolbox*” is available at <http://dustem.astro.umd.edu> and contains downloadable FIR lines diagnostic information about PDRs. The tool has been created by L. Mundy, M. Wolfire, S. Lord and M. Pound, and it is based on the new PDR models of Kaufman et al. (1999).

⁶The ISO archive is available at <http://pma.iso.vilspa.esa.es>

⁷Copious [OI]63 μ m can also be produced in non-dissociative shocks. In this case however, the presence of H₂ would allow the incorporation of O into water, via the chain of endothermic reactions $O + H_2 \rightarrow OH + H$ and $OH + H_2 \rightarrow H_2O + H$. This chain has an activation energy of $T \sim 220$ K, lower than the H₂ temperature estimated from the rotational lines (between 540 and 670 K, see Table 3); we conclude that the observed [OI]63 μ m emission cannot originate in C-shocks.

TABLE 4
Cooling rates^a

Species	HH 7	HH 10	SVS 13	RL 1	RL 2
[OI]63 μ m	4.8		6.6	4.0	
CO	2.0		3.0	1.4	
H ₂ O	0.7		0.7	–	
H ₂	2.3	1.9	1.6	1.7	1.6
[SiII]34.8 μ m	0.13	0.25	0.27	0.20	–

^a Units of $10^{-2} L_{\odot}$.

as weights to estimate the [OI]63 μ m cooling intrinsic to HH 7. We conservatively assign to HH 8 and HH 9 the same [SiII]34.8 μ m flux measured toward HH 7, and we also consider that the weighting of the LWS beam profile decreases the contribution of HH 8-9 and HH 10 to the [OI]63 μ m measured on the HH 7 pointing by 10% and 50%, respectively. Similar estimates can be done for the SVS 13 pointing, where again HH 10 contributes at a 50% level. The HH 11's contribution does not need to be disentangled since it also contributes to the [SiII]34.8 μ m line of SVS 13. No correction is required for the RL 1+2 pointing. Taking the above into account, we obtain [OI]63 μ m/[SiII]34.8 μ m line ratios between 15 and 20, suggesting a pre-shock density $n_0 \sim 10^4 \text{ cm}^{-3}$ (HM89). The models can also reproduce the absolute fluxes, provided that the emission solid angles are $\sim 5''$ in diameter with filling factor of 1; more intense OI and SiII lines on the central position are likely due to slightly larger solid angles and/or filling factors.

As concerns molecular cooling the main contribution to H₂ emission in J-shocks is predicted (HM89) to come from material excited by FUV or H₂-formation pumping. Indeed, Fernandes & Brand (1995) propose a fluorescent origin for the near-IR H₂ lines toward HH 7. For the (0-0)S lines however, the predicted line ratios are not reproduced by the observations. In particular the S(7) line, which is predicted to be always brighter than the S(5) line irrespectively of pre-shock density and shock velocity, is not detected at all in our SWS spectra⁸.

6.2. C-shocks

When interpreted in terms of non-dissociative shock, the pure rotational H₂ lines provides a sensitive probe for the shock velocity, given the four orders of magnitudes of dynamical range spanned by their line ratios. This is shown in Fig. 5, which presents the observed H₂ line ratios superimposed on a grid of C-shock models from Kaufman & Neufeld (1996).

Our observations seem to place quite stringent boundaries to the shock velocity, $15 \lesssim v_s \lesssim 20 \text{ km s}^{-1}$. The corresponding gas temperature, $\sim 600 \text{ K}$ (Kaufman & Neufeld 1996), is in good agreement with the values derived using simple LTE analysis (Sect. 4), as expected since the molecular gas is collisionally heated by the C-shock front. Observed absolute fluxes can also be reproduced by the model as long as the emission solid angle does not exceed few arcsecs in diameter. We note that such a low velocity shock would also produce very faint S(6) and S(7) lines. Once the shock velocity is determined, we can use the CO/H₂ cooling ratio to estimate the pre-shock density. Fig. 6 presents such a diagnostic diagram.

The CO line fluxes in the three LWS pointings should be corrected for contamination by the other HH objects. In similar way as for the [OI]63 μ m/[SiII]34.8 μ m ratio, we use the H₂ coolings in different positions as weights to split the individual contributions to the CO cooling. The corrected cooling ratios are reported as dashed lines in Fig. 6. We see that a shock velocity $15 \lesssim v_s \lesssim 20 \text{ km s}^{-1}$ would correspond to a pre-shock densities of $n_0 \sim 10^4 \text{ cm}^{-3}$ for HH 7 and

⁸The above mentioned ISOCAM-CVF observations (at lower spectral resolution than the SWS) actually detected the S(7) but with a flux about 4 times lower than the S(5) line flux, compatibly with our SWS upper limits on the S(7) line (Noriega-Crespo et al. 2000).

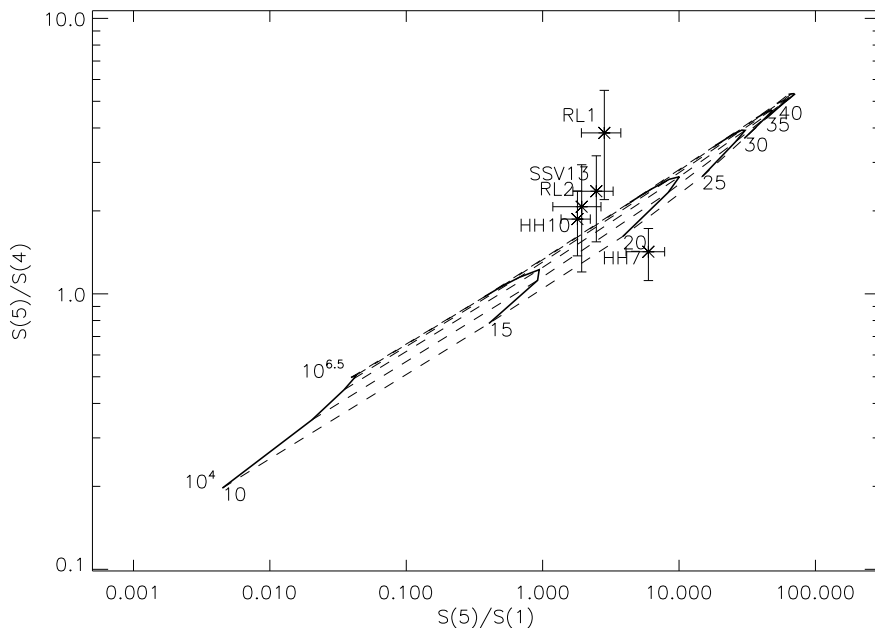


FIG. 5.— C-shock diagnostic ratios for the H_2 pure rotational lines. The solid and dashed lines represent iso-density and iso-velocity levels respectively. The levels are labeled in cm^{-3} (powers of ten) and in km s^{-1} . The crosses represent the H_2 line ratios for the five positions observed with the SWS.

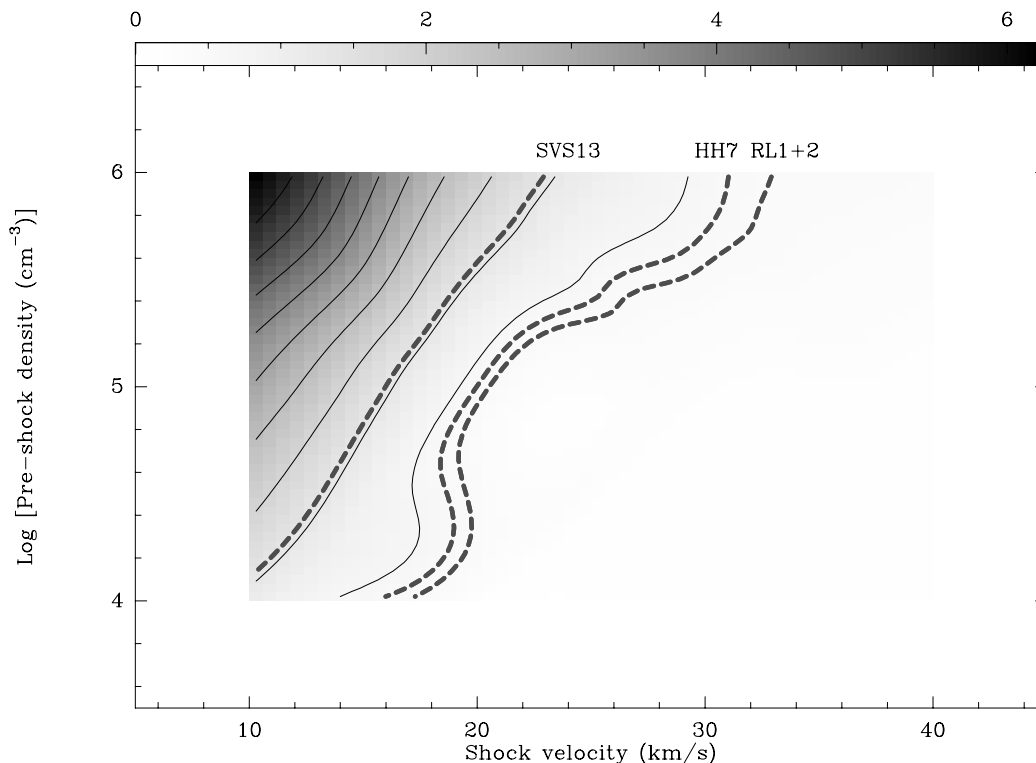


FIG. 6.— CO/H_2 cooling ratio as predicted for C-shock models (Kaufman & Neufeld 1996) as a function of pre-shock density and shock velocity. The dashed lines indicate the values observed in the different LWS pointings.

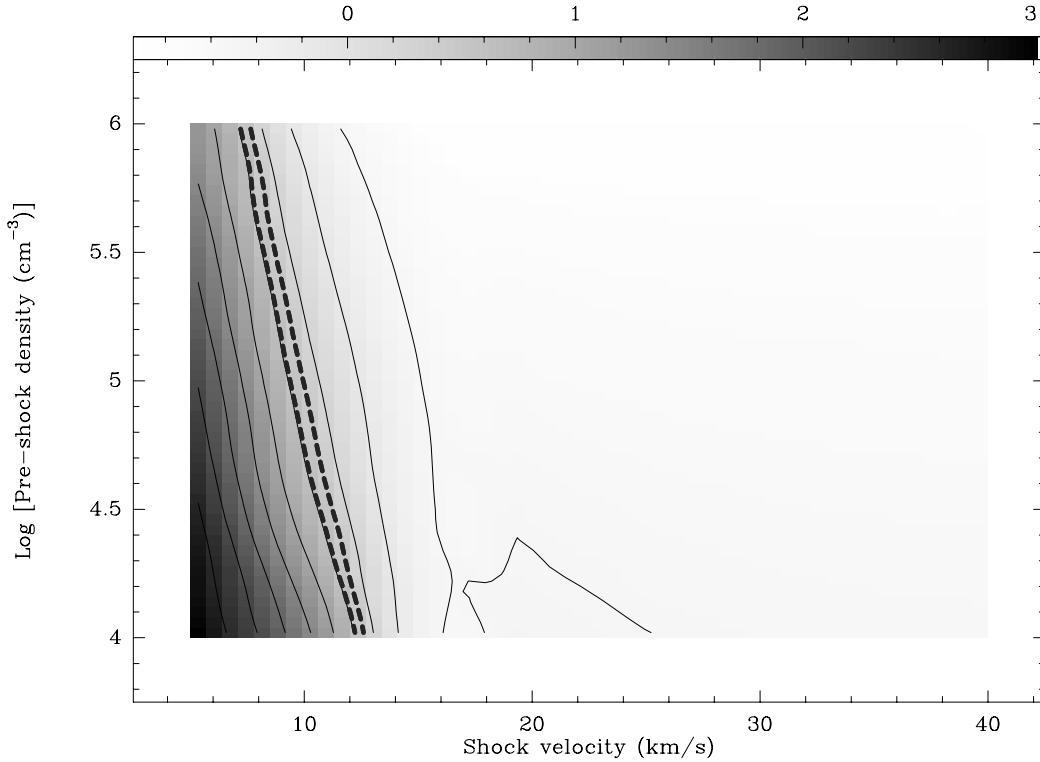


FIG. 7.— Decimal logarithm of the CO/H₂O cooling ratio as predicted for C-shock models (Kaufman & Neufeld 1996) as a function of pre-shock density and shock velocity. The dashed lines indicate the values observed toward HH 7 and SVS 13 (water emission was not detected toward RL 1+2).

RL 1+2, and $n_0 \sim 10^5 \text{ cm}^{-3}$ for SVS 13.

Water is an important diagnostic for C-shock models. H₂O cooling is a fast function of the shock velocity since free atomic oxygen in the post-shock gas is expected to be incorporated into water as soon as the temperature rises above $\sim 200 \text{ K}$, roughly corresponding to $v_s \sim 10 \text{ km s}^{-1}$ (Draine, Roberge & Dalgarno 1983, Kaufman & Neufeld 1996). In our case then, where the temperature is $\sim 600 \text{ K}$, cooling via H₂O rotational transitions is expected to be dominant with respect to that of CO. Instead, the diagnostic diagram in Fig. 7 shows that the observed CO/H₂O cooling ratio is consistent with shock velocities $v_s \lesssim 12 \text{ km s}^{-1}$, which cannot justify the observed H₂ temperatures. This suggests that most of the expected gas phase water is missing. We will propose an explanation for this result in Sect. 7.1

7. THE SHOCKS AND THE HERBIG-HARO OBJECTS

We have shown that HH 7-11 is a complex region where different line emission mechanisms are simultaneously at work. Notwithstanding the poor spatial resolution of our data, the variety of different spectral signatures detected allow us to

draw the following physical scenario of the region.

7.1. HH 7

Starting from HH 7, the C-shock conditions diagnosed by the molecular emission clearly require the presence of a magnetic field $\mathbf{B}_0 \perp \mathbf{v}_{sC}$ (Draine 1980), where \mathbf{v}_{sC} is the shock velocity of the C component. Assuming the standard scaling law (Draine 1980) for the value of B_0

$$B_0 \sim b n_0^{0.5} \mu\text{G} \quad (1)$$

where $b \sim 1$ in the interstellar medium, the estimated $n_0 \sim 10^4 \text{ cm}^{-3}$ pre-shock density for the C-shock component on HH 7 gives $B_0 \sim 100 \mu\text{G}$. Variations of a factor 3 in each direction are nevertheless possible, since b can vary between 0.3 and 3 in molecular clouds (HM89). For similar B_0 and n_0 , Draine, Roberge & Dalgarno (1983) have shown that the C \rightarrow J transition occurs at $v_s \sim 50 \text{ km s}^{-1}$, similar to the upper limit set on v_{sJ} (the J-shock velocity) by our observations. This means that a significant \mathbf{B}_0 component transverse to \mathbf{v}_{sJ} would smooth the shock front to a C type or, equivalently, that our observed J-shock component can only exist as long as $\mathbf{v}_{sJ} \parallel \mathbf{B}_0$. When

the bowshock-like morphology of HH 7 is also considered, as revealed by HST NICMOS $2.12\mu\text{m}$ images (A. Cotera, priv. comm.), then a very simple scenario emerges where HH 7 is immersed in a \mathbf{B}_0 roughly parallel to the flow axis. At the tip of the bow $\mathbf{v}_s \sim \|\mathbf{B}_0$ and J-shock conditions are present; [SiII] $34.8\mu\text{m}$ and most of [OI] $63\mu\text{m}$ flux arise from this region, and favourable conditions also exist to originate the ‘‘hot’’, $T \sim 2100$ K, H_2 emission detected by Gredel (1996). Along the sides of the bow, \mathbf{v}_s becomes nearly perpendicular to \mathbf{B}_0 , creating favourable conditions for C-type shocks. This picture also provides a plausible explanation to the problem of the missing water: the water is actually produced in the C-shocks, but rapidly condenses onto dust grains and disappears from the gas-phase. This possibility is suggested by the recent discovery with ISO-LWS (Molinari et al. 1999) of crystalline water ice toward HH 7. The deduced water abundance (in solid state form) is comparable to the interstellar oxygen abundance, which is what the models would predict for gas-phase water in C-shocks; furthermore, the fact that the ice is in crystalline form requires grain temperatures of the order of 100 K, only attainable in dissociative shocks (HM89; Draine, Roberge & Dalgarno 1983). After being heated, the grains would be efficiently transported in the post C-shock regions along the \mathbf{B} lines, directed parallel to the flow. For the gas parameters we derived, the grains are efficiently coupled to the magnetic field and are not significantly decelerated by collisions with the neutrals (Draine, Roberge & Dalgarno 1983).

7.2. HH 10

From the viewpoint of the line emission properties, HH 10 and HH 7 appear very similar objects. Although no LWS data were specifically collected toward HH 10, the H_2 and the [SiII] $34.8\mu\text{m}$ lines still argue in favour of a dual J+C shock nature. From the morphological point of view, HH 10 appears as an irregular blob in the $2.12\mu\text{m}$ image of Fig. 1. Higher spatial resolution images in $\text{H}\alpha$ and [SiI] $6717+31\text{\AA}$ from HST (unpublished archival data) resolved HH 10 into a double filamentary structure whose N-S orientation does not appear to be related to the flow direction. However, the $\text{H}\alpha$ /[SiI] $6717+31\text{\AA}$ emission ratio is higher in the NW part of this HH object, facing toward SVS 13. A higher ratio implies higher excitation (stronger shocks) conditions, which are likely to be traced

by the [SiII] $34.8\mu\text{m}$ line and by the ‘hot’, $T \sim 2200$ K, H_2 component (Gredel 1996). If we assume that \mathbf{B}_0 maintains its direction downstream along the flow, as suggested for HH 7 (see above), then we speculate that the morphology of HH 10 could correspond to irregularities or corrugations in the shocked walls of the cavity which is excavated by the flow. Such irregularities might originate from instabilities at the flow-cavity interface, as proposed by Liseau, Sandell & Knee (1988), although there are no detailed numerical simulations of the process.

7.3. HH 11 and SVS 13

The interpretation for HH 11 and SVS 13 is more complicated because both sources are contained in the fields of view of the SWS and LWS instruments. Pre-shock densities $n_0 \sim 10^5 \text{ cm}^{-3}$ are here found for the C component; this is a factor ten higher than in the other positions of the flow, which is not surprising given the close proximity of the origin of the flow. In these conditions the magnitude of the magnetic field (Eq. 1) could range from $\sim 300\mu\text{G}$ to $\sim 1\text{mG}$. Such high B_0 values have been claimed by Hartigan, Curiel & Raymond (1989) to justify the relative faintness of HH 11 in $2.12\mu\text{m}$ H_2 images (see also Fig. 1). The possibility that FIR line emission toward SVS 13 arises in a collapsing envelope around is not relevant here because the predicted [OI] $63\mu\text{m}$ line flux (Ceccarelli, Hollenbach & Tielens 1996) is about 30 times lower than actually observed, while CO and H_2O lines are below the detection limit for the present observations. Finally, there is the possibility that a fraction of the line fluxes measured with the LWS originates from the recently discovered embedded outflow source SVS 13B (Bachiller et al. 1998).

7.4. The Red-shifted Lobe

[OI] $63\mu\text{m}$, [OI] $145\mu\text{m}$ and [SiII] $34.8\mu\text{m}$, together with a complement of H_2 and CO lines, have been detected toward the receding lobe, and define shock conditions which are not dramatically different from those present on the blue lobe. It is well known that no optical emission is detected toward the red lobe, and also published images in the H_2 $2.12\mu\text{m}$ line (Fig. 1, Garden et al. 1990, Hodapp & Ladd 1995) clearly show fainter emission there. Higher values of dust extinction with respect to the blue lobe have been

invoked as an explanation for this asymmetry. Our observations, which trace similar shock conditions for the two lobes, tend to support this possibility.

8. THE SHOCKS AND THE MOLECULAR OUTFLOW

If J-shocks between stellar winds and ambient material are responsible for the acceleration of the molecular outflow, a correlation (Hollenbach 1985) is expected between the outflow mass loss rate and the flux of the [OI]63 μ m line, which is the dominant coolant in such shocks. The predicted mass loss rate, based on the observed [OI]63 μ m cooling from HH 7, is $4.8 \times 10^{-6} M_{\odot} \text{ yr}^{-1}$ (see also Cohen et al. 1988, Ceccarelli et al. 1997), in good agreement with the mass loss rate estimated by Lizano et al. (1988, see also Rodriguez et al. 1990) for the fast HI wind believed to be responsible for the acceleration of the slow CO outflow (Snell & Edwards 1981). This fast neutral wind was also confirmed with CO observations by Bachiller & Cernicharo (1990).

Assuming momentum balance at the interface between the the wind and the ambient medium, Davis & Eisloffel (1995, 1996) derived a simple relationship between the mechanical power of the wind L_w and the power radiated by the shock L_{rad} :

$$\frac{L_{rad}}{L_w} = \frac{v_s}{v_w} \left[1 - \frac{v_s}{v_w} \right]^2 \quad (2)$$

Since the working surfaces where the winds impact the medium are traced by the J-shocks, we make the assumption $L_{rad} \sim L_{OI} + L_{SiII} + L_{H_2-vib}$. The total cooling due to the near-IR H₂ vibrational lines measured by Gredel (1996) along the flow is $\sim 5 \times 10^{-3} L_{\odot}$; we assume a slit width of few arcsecs, so we will conservatively multiply the observed value by 10 to allow for the extension of the HH objects. We estimate the mechanical power of the HI wind according to:

$$L_w = \frac{1}{2} \frac{M_w v_w^2}{\tau_{dyn}} \quad (3)$$

Using the HI parameters from Lizano et al. (1988), we obtain $L_w \sim 1.9 L_{\odot}$. Eq. (2) then provides $v_s/v_w \sim 0.6$, or $v_{s,J} \sim 36 \text{ km s}^{-1}$ for an average HI wind velocity of $v_w \sim 60 \text{ km s}^{-1}$ (Lizano et al. 1988), in excellent agreement with our results.

9. SUMMARY

The HH 7-11 flow, together with its red-shifted counterpart and SVS 13 (the candidate exciting source) have been studied via atomic, ionic and molecular spectroscopy. A complex scenario emerges, where:

1. we have detected atomic ([OI]63 μ m, [OI]145 μ m), ionic ([CII]158 μ m, [SiII]34.8 μ m) and molecular (H₂, CO and H₂O) lines along the flow (both lobes) and toward SVS 13.
2. the low-excitation shock nature of the HH nebulosities along the flow is confirmed. Spectral signatures of C and J shocks are ubiquitously found along the HH 7-11 flow and its red-shifted counterpart. Our estimates for the shock velocities are $v_{s,J} \lesssim 40-50 \text{ km s}^{-1}$ and $15 \lesssim v_{s,C} \lesssim 20 \text{ km s}^{-1}$. The pre-shock density is $\sim 10^4 \text{ cm}^{-3}$ toward the blue and the red lobe; for the C component only, we find $n_0 \sim 10^5 \text{ cm}^{-3}$ at the location of SVS 13.
3. there is indirect evidence for an ordered **B** field oriented parallel to the direction of the flow. The magnitude of the magnetic field is $B_0 \sim 100 \mu\text{G}$ on the lobes, increasing to $\sim 300 \mu\text{G}$ at the position of the flow origin; these figures, however, can vary of a factor 3 in each direction.
4. the gas-phase in the post C-shock region is deficient in H₂O. We presented evidence that this may be due to freezing onto warm grains processed through the J-shock front and traveling downstream along the magnetic field lines.
5. the asymmetry in optical and NIR properties among the two lobes of the outflow is probably not caused by different pre-shock densities or shock velocities, supporting the hypothesis of higher extinction values toward the red lobe.
6. the total J-shock cooling is compatible with the molecular outflow being accelerated by the fast neutral wind detected in HI and CO.
7. the whole flow area appears to be associated with a faint PDR illuminated by BD

+30° 549, the source responsible for the illumination of the whole NGC 1333 nebula.

We thank L. Testi and M. Cecere for their assistance with the observations and data reduction of the H₂ 2.12μm image presented in Fig. 1. The staff of the Mt. Palomar 60" telescope is also acknowledged. We also thank an anonymous referee

whose comments improved the paper, and L.F. Rodriguez for his comments on an early version of this manuscript. The ISO Spectral Analysis Package (ISAP) is a joint development by the LWS and SWS Instrument Teams and Data Centers. Contributing institutes are CESR, IAS, IPAC, MPE, RAL and SRON.

REFERENCES

- Aspin, C., Sandell, G. Russell, A.P.G. 1994, *A&AS*, 106, 165
- Bachiller, R., Cernicharo, J. 1990, *A&A*, 239, 276
- Bachiller, R., Gilloteau, S., Gueth, F., Tafalla, M., Dutrey, A., Codella, C., Castets, A. 1998, *A&A*, 339, 49
- Bally, J., Devine, D., Reipurth, B. 1996, *ApJ*, 473, 49
- Black, J.H., Dalgarno, A. 1976, *ApJ*, 203, 132
- Böhm, K.H., Solf, J. 1990, *ApJ*, 348, 297
- Böhm, K.H., Brugel, E.W., Olmsted, E. 1983, *A&A*, 125, 23
- Cardelli, J.A., Meyer, D.M., Jura, M., Savage, B.D. 1996, *ApJ*, 467, 334
- Carr, J.S. 1993, *ApJ*, 406, 553
- Caux, E., et al. 2000 (in preparation).
- Ceccarelli, C., Hollenbach, D., Tielens, A.G.G.M. 1996, *ApJ*, 499, 294
- Ceccarelli, C., Haas, M.R., Hollenbach, D., Rudolph, A.L. 1997, *ApJ*, 476, 771
- Ceccarelli, C., Caux, E., White, G.J., et al. 1998, *A&A*, 331, 372
- Cernicharo, J., Bachiller, R., González-Alonso, E. 1996, *A&A*, 305, L5
- Cernis, K. 1993, *Baltic Astronomy*, 2, 214
- Clegg, P.E., Ade, P.A.R., Armand, C., et al. 1996, *A&A*, 315, L38
- Cohen, M., Hollenbach, D.J., Haas, M.R., Erickson, E.F. 1988, *ApJ*, 329, 863
- Dabrowski, I. 1984, *Can. J. Phys.*, 62, 1639
- Davis, C.J., Eislöffel, J. 1995, *A&A*, 300, 851
- Davis, C.J., Eislöffel, J. 1996, *A&A*, 305, 694
- de Graauw, T., Haser, L.N., Beintema, D.A., et al. 1996, *A&A*, 315, L49
- Draine, B.T. 1980, *ApJ*, 241, 1021
- Draine, B.T., Roberge, W.G., Dalgarno, A. 1983, *ApJ*, 264, 485
- Eislöffel, J., Gunther, E., Hessman, F.V., Mundt, R., Poetzelt, R., Carr, J.S., Beckwith, S., Ray, T.P. 1991, *ApJ*, 383, 19
- Everett, M.E. 1997, *ApJ*, 478, 246
- Fernandes, A.J.L., Brand, P.J.L. 1995, *MNRAS*, 274, 639
- Garden, R.P., Russell, A.P.G., Burton, M.G. 1990, *ApJ*, 354, 232
- Giovanardi, C., Lizano, S., Natta, A., Evans, N.J., Heiles, C. 1992, *ApJ*, 397, 214
- Goodrich, R.W. 1986, *AJ*, 92, 885
- Gredel, R. 1994, *A&A*, 292, 580
- Gredel, R. 1996, *A&A*, 305, 582
- Grossman, E.N., Masson, C.R., Sargent, A.I., et al. 1987, *ApJ*, 320, 356
- Habing, H.J. 1968, *Bull. Astr. Inst. Netherlands*, 19, 421
- Hartigan, P., Curiel, S., Raymond, J. 1989, *ApJ*, 347, 31
- Harvey, P.M., Wilking, B.A., Joy, M. 1984, *ApJ*, 278, 156
- Herbig, G.H. 1974, *Draft Catalog of Herbig-Haro Objects*, *Lick Obs. Bull. No. 658*
- Herbig, G.H., Jones, B.F. 1983, *AJ*, 88, 1040
- Hodapp, K.-W., Ladd, E.F. 1995, *ApJ*, 453, 715
- Hollenbach, D. 1985, *Icarus*, 61, 36
- Hollenbach, D., McKee, C.F. 1989, *ApJ*, 342, 306 (HM89)
- Hollenbach, D., Takahashi, T., Tielens, A.G.G.M. 1991, *ApJ*, 377, 192
- Kaufman, M.J., Neufeld, D.A. 1996, *ApJ*, 456, 611
- Kaufman, M.J., Wolfire, M.G., Hollenbach, D., Luhman, M.L. 1999, *ApJ*, 527, 795
- Kemper, C., Spaans, M., Jansen, D.J., Hogerheijde, M.R., van Dishoeck, E.F., Tielens, A.G.G.M. 1999, *ApJ*, 515, 649
- Kessler, M.F., Steinz, J.A., Anderegg, M.E., et al. 1996, *A&A*, 315, L27
- Lefloch, B., Castets, A., Cernicharo, J., Langer, W.D., Zylka, R. 1998, *A&A*, 334, 269
- Liseau, R., Sandell, G., Knee, L.B.G. 1988, *A&A*, 192, 153
- Liseau, R., Lorenzetti, D., Molinari, S. 1992, *A&A*, 253, 119
- Liseau, R., White, G.J., Larsson, B., et al. 1999, *A&A*, 344, 342
- Lizano, S., Heiles, C., Rodriguez, L.F., Koo, B.C., Shu, F.H., Hasegawa, T., Hayashi, S., Mirabel, I.F. 1988, *ApJ*, 328, 763
- Loren, R.B. 1976, *ApJ*, 209, 466
- Masson, C.R., Chernin, L.M. 1993, *ApJ*, 414, 230
- Mehring, D.M. 1996, *ApJ*, 462, 355
- Molinari, S., Liseau, R., Lorenzetti, D. 1993, *A&AS*, 101, 53
- Molinari, S., Saraceno, P., Nisini, B., et al. 1998, "Star Formation with the Infrared Space Observatory" (eds. Yun J. and Liseau R.), *ASP Conference Series* 132, 390
- Molinari, S., Ceccarelli, C., White, G.J., Saraceno, P., Nisini, B., Giannini, T., Caux, E. 1999, *ApJ*, 521, L71
- Murphy, D.C., Persson, S.E., Pahre, M.A., Sivaramakrishnan, A., Djorgovski, S.G. 1995, *PASP*, 107, 1234
- Nisini, B., Benedettini, M., Giannini, T., et al. 1999, *A&A*, 350, 520
- Noriega-Crespo, A., Molinari, S., Ali, B., Cabrit, S., & Cernicharo, J. 2000 (in preparation).
- Raga, A.C. 1991, *AJ*, 101, 1472
- Raga, A.C., Canto, J., Calvet, N., Rodriguez, L.F., Torrelles, J.M. 1993, *A&A*, 276, 539
- Reipurth, B. 1994, *A General Catalog of Herbig-Haro Objects* (<ftp://ftp.hq.eso.org/pub/Catalogs/Herbig-Haro>)
- Rieke, G.H., Lebofsky, M.J. 1985, *ApJ*, 288, 618
- Rodriguez, L.F., Lizano, S., Canto, J., Escalante, V., Mirabel, I.F. 1990, *ApJ*, 365, 261
- Snell, R.L., Edwards, S. 1981, *ApJ*, 251, 103
- Solf, J., Böhm, K.H. 1987, *AJ*, 93, 1172
- Stapelfeldt, K.R. 1991, Ph. D. Thesis, California Institute of Technology
- Strom, S.E., Grasdalen, G.L., Strom, K.M. 1974, *ApJ*, 191, 111
- Strom, S.E., Vrba, F.J., Strom, K.M. 1976, *AJ*, 81, 314
- Swinyard, B.M., Burgdorf, M.J., Clegg, P.E., Davis, G.R., Griffin, M.J., et al. 1998, *Proc. SPIE*, 3354, 888
- Tielens, A.G.G.M., Hollenbach, D. 1985, *ApJ*, 291, 722
- Timmermann, R., Bertoldi, F., Wright, C.M., Drapatz, S., Draine, B.T., et al. 1996, *A&A*, 315, L284